International Journal of Astrobiology 14 (2): 165–172 (2015)
doi:10.1017/S1473550414000329

Stellar statistics along the ecliptic and the impact on the K2 mission concept

Andrej Prša[1,2], Annie Robin[3] and Thomas Barclay[4,5]

[1]*Department of Astrophysics and Planetary Science, Villanova University, 800 E Lancaster Ave, Villanova, PA 19085, USA*
[2]*Jeremiah Horrocks Institute, University of Central Lancashire, Preston PR1 2HE, UK*
e-mail: aprsa@villanova.edu
[3]*Institute Utinam, CNRS UMR6213, Université de Franche-Comté, OSU THETA de Franche-Comté-Bourgogne, Besançon, France*
[4]*NASA Ames Research Center, M|S 244-30, Moffett Field, CA 94035, USA*
[5]*Bay Area Environmental Research Institute, 596 1st Street West, Sonoma CA 95476, USA*

Abstract: K2 is the mission concept for a repurposed *Kepler* mission that uses two reaction wheels to maintain the satellite attitude and provide ∼81 days of coverage for ten 105 deg^2 fields along the ecliptic in the first 2.5 years of operation. We examine stellar populations based on the updated Besançon model of the Galaxy, comment on the general properties for the entire ecliptic plane, and provide stellar occurrence rates in the first six tentative K2 campaigns grouped by spectral type and luminosity class. For each campaign we distinguish between main the sequence stars and giants, and provide their density profile as a function of galactic latitude. We introduce the crowding metric that serves for optimized target selection across the campaigns. For all main sequence stars we compute the expected planetary occurrence rates for three planet sizes: 2–4, 4–8 and 8–32 $R_\oplus$ with orbital periods up to 50 days. In conjunction with Gaia and the upcoming Transiting Exoplanet Survey Satellite and Plato missions, K2 will become a gold mine for stellar and planetary astrophysics.

Received 24 March 2014, accepted 25 July 2014, first published online 28 August 2014

Key words: extrasolar planets, *Kepler*, stellar populations.

Introduction

Space-borne missions CoRoT (Baglin 2003) and *Kepler* (Borucki *et al.* 2010) revolutionized stellar and planetary physics by providing us with ultra-precise photometric data of ∼ 30 ppm. The duty cycle of observations exceeded 90% and, for the first time, we had nearly uninterrupted time coverage of over 200 000 objects. The two missions predominantly catered for two overlapping communities, the exoplanetary science and asteroseismology. The detection of extra-solar planets using the transit method boosted their numbers from dozens to nearly 5000 (Batalha *et al.* 2013; Burke *et al.* 2014; Rowe *et al.* 2014) and the number is growing still as data are being mined. At the same time, asteroseismology witnessed an explosion in novel techniques and exciting new results (Chaplin *et al.* 2011), ranging from main sequence B stars (Papics 2013) to solar-like oscillations in red giants (Gaulme *et al.* 2013). The overlap between the fields is provided using asteroseismic techniques that provide fundamental properties of planet candidate host stars, which in turn enable exoplanet researchers to obtain precise fundamental properties of planets (Huber *et al.* 2013). Unfortunately, CoRoT suffered from a computer failure in November 2012 and attempts to restore it ceased in June 2013. *Kepler* lost a second reaction wheel in May 2013, causing the telescope to go to a prolonged point rest state; attempts to bring *Kepler* back to operational state ceased in July 2013. However, this did not imply that *Kepler* is retired; a proposal to use solar photon pressure to balance a two-wheel *Kepler* satellite enabled a continued operation. For this balancing to work, the telescope must point approximately in the direction of the ecliptic, so the observations of the initial *Kepler* field are no longer possible. The spacecraft can hold pointing within +50° and −30° of its velocity vector in the orbital plane (approximately the ecliptic), with the two remaining reaction wheels holding the cross-boresight pointing steady. The spacecraft roll is minimized through regular thruster firing windows. The satellite can remain stable in roll for up to 81 days with a fuel budget that allows for a 2–3-year mission duration. A new mission concept, K2 (Howell *et al.* 2014), builds on this engineering constraint. The science case arose from the community response to the whitepaper call for the repurposed mission and the concept was submitted to NASA HQ for the 2014 Senior Review (pending at the time of this writing). The first engineering observations utilizing the K2 mission design concept were obtained in October 2013 and the first full campaign-length test began in March 2014. This field lies in the direction near the galactic anti-centre ($\alpha_{2000} = 6$ h 33 min 11.1 s, $\delta_{2000} = 21°35'16''$) and includes M35 and NGC 2158. The subsequent fields will be observed for 83 days; the duration is limited by solar illumination. If selected, K2 will observe upwards of 40 000–80 000 targets over the first year in four distinct fields.

Kepler is a 0.95 m telescope with a 105 deg^2 field of view. The early science commissioning run from October 2013 to February 2014 showed that the precision of K2 photometry for a $V = 12$ star is ~ 400 ppm for the 30 min long cadence exposure and ~ 80 ppm for an integrated 6-h exposure. Since then, further optimization reduced the noise for bright stars to under 60 ppm (D. Caldwell, NASA Ames; private communication). The precision primarily depends on the spacecraft attitude jitter; the point spread function (PSF) of the K2 field is within 5% of the original *Kepler* PSF, and the degradation in precision due to a solar-induced drift is approximately fourfold (Howell *et al.* 2014). Early science demonstration for WASP-28, a hot Jupiter orbiting a Sun-like star in a 3.4-day orbit, corresponds to a 6-h integrated noise level of 84 ppm.

This work employs the updated Besançon model of the Galaxy (hereafter BGM; Robin *et al.* 2003; Robin *et al.* 2014) to simulate stellar populations along the ecliptic. The K2 mission has the potential for observing $\sim 250\,000$ stars, and selecting targets hinges crucially on the representative population within each K2 field. The goal of this paper is to study the bulk properties and to serve as a guide to stellar populations along the ecliptic. This information can be used to better understand different populations from which the K2 targets are drawn, and to enable debiasing of any results that stem from statistical analyses of K2 campaigns.

The updated Besançon model

The BGM (Robin *et al.* 2003) has served as one of the premier stellar population models. The model is by no means the only choice – alternatives being TRILEGAL (Girardi *et al.* 2005), the models of Ng *et al.* (1997) and Vallenari *et al.* (1999), as well as the BGM-derived approach Galaxia (Sharma *et al.* 2011). The BGM and TRILEGAL produce equivalent results at high galactic latitudes despite slight differences in model parameters, which is a consequence of the model degeneracies. However, the BGM tends to produce more realistic star counts in the bulge region because the bar and the bulge are modelled by distinct populations in BGM, but not in TRILEGAL (Schultheis, private communication).

The BGM model has been tested extensively over the years by comparisons to star counts, colour distributions and other statistics. Most recent comparisons with 2MASS and SDSS surveys have been presented in Robin *et al.* (2012) and in Robin *et al.* (2014). It shows that the model is reliable at the level of a few per cent in most fields at medium and high latitudes for visual magnitudes larger than 14. The uncertainties are larger close to the galactic plane due to extinction, where it can reach up to 50% in fields where extinction is large, in star forming regions, in spiral arms and close to the Galactic centre. The spiral structure is under investigation and will be included in the near future. The model has been shown to overestimate the number of stars at the bright end ($V < 12$) due to the use of a constant star formation rate.

Here we use the BGM described in Robin *et al.* (2003), updated by Reylé *et al.* (2009) for the warp and flare parameters, by Robin *et al.* (2012) for the bulge and bar region, by Robin *et al.* (2014) for the thick disc and halo shapes. The extinction model used is based on Marshall *et al.* (2006), where we use the standard value for the total-over-selective extinction (R_V) of 3.1 for all lines of sight. We further use the Cardelli *et al.* (1989) extinction law to convert the *K*-band extinction map to the *Kp* band.

The model features four stellar populations: a thin disc, a bar, a thick disc and a spheroid. The star formation rate is constant over 10 Gyr for the thin disc population and is assumed to be a single burst in other populations with ages of 8, 12 and 14 Gyr, respectively. Each population has it own density law that were derived from wide survey data fits. Basel 3.1 (Westera *et al.* 1999) atmosphere models are used to compute the photometry in various systems (Johnson-Cousins, 2MASS, Spitzer, GALEX, UVIT).

This version of BGM does not take binary and multiple stars into account, but a new revision by Czekaj *et al.* (2014) builds in binary populations as well, following the formalism of Arenou (2011). For the purpose of this simulation only single stars are generated, so for remote populations the luminosity functions represent more systems than single stars. There are also no open clusters in the simulation. We estimate the prediction uncertainty due to these drawbacks in Conclusions.

Stellar statistics

The original *Kepler* mission observed a *biased* set of targets that comprised mainly FGK main-sequence stars, as those hold the highest promise for detecting extra-solar planets. Thus, any stellar population studies would be strongly hampered by this selection effect and any conclusions drawn from the *Kepler* dataset would need to be corrected substantially. Furthermore, there are $\sim 600\,000$ objects in the original *Kepler* field of view that are brighter than $Kp = 16$, but the *Kepler* target list can only hold $\sim 150\,000$ due to telemetry restrictions. Thus, three quarters of viable targets had to be dropped. Finally, all red giants identified in early *Kepler* data were removed from the target list and all subsequent observations have ceased. With the initial selection geared to exoplanet science, subsequent target list pruning and a number-limited instead of magnitude-limited sample, the original *Kepler* mission was not well suited for stellar population studies. Nevertheless, the effects of stellar population variation were reported by Prša *et al.* (2011, Fig. 12 therein), where a decreasing number of eclipsing binaries was observed with the increasing galactic latitude. This was a small effect, though, due to the fixed field. K2, on the other hand, will be much better suited for such studies, as we demonstrate next, since it covers a span of $-70°$ to $+70°$ in galactic latitude.

We ran the new BGM model for 20 distinct fields along the ecliptic. The fields are $20° \times 20°$ in size and rectilinear in equatorial coordinates; the resolution element is 1 deg^2. The fields are then transformed into galactic and ecliptic systems and star counts are performed for each 1 deg^2 cell. Figure 1 depicts the number of stars in each cell for all 20 fields, and the original *Kepler* field. The simulated stars range from $Kp = 7$–17

https://doi.org/10.1017/S1473550414000329 Published online by Cambridge University Press

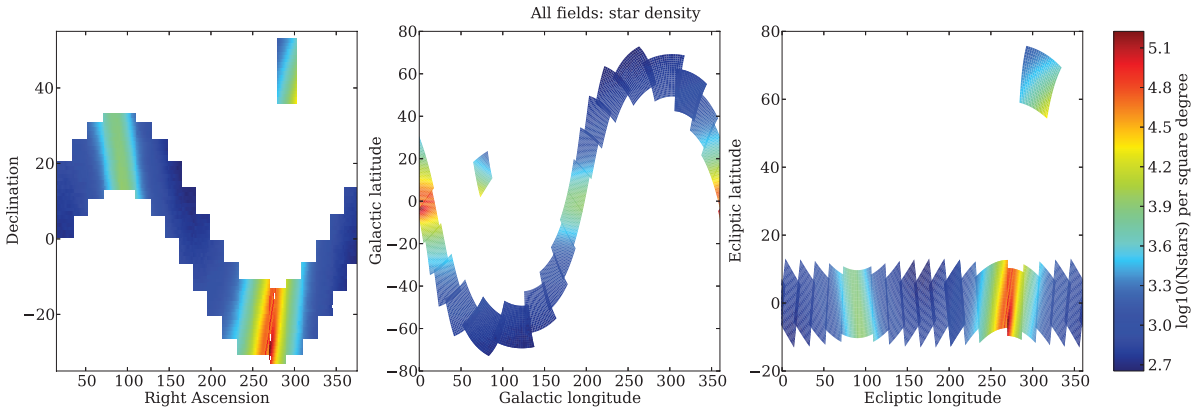

Fig. 1. Star counts (in log10 scale, $Kp = 7$–17) in equatorial, galactic and ecliptic coordinates for 20 fields along the ecliptic. The counts are computed using the 2014 Besançon model of the Galaxy and range from ~ 500 to $\sim 160\,000$ stars per deg^2. The original *Kepler* field is included for comparison purposes.

and cover all spectral types and luminosity classes in this magnitude range. All parameters of the model (used evolutionary tracks, atmosphere models, age-metallicity and age-velocity relations, the extinction model and radial scale length) can be found in Czekaj *et al.* (2014).

It is instructive to review the predictions of BGM for single star populations. Figure 2 depicts nine principal parameters of the stellar populations along the ecliptic in the $Kp = 7$–17 magnitude range. Below we provide a brief commentary on each.

Distances: The distance to the targets along the ecliptic is up to 2 kpc, except that which is close to the galactic plane, where it climbs above ~ 3 kpc. Baade's window, the largest transparent area towards the galactic bulge ($\alpha_{2000} = 18$ h 03 min 36 s, $\delta_{2000} = -30°02'00''$), corresponds to the largest distances, upwards of 6 kpc, where we can see the old, evolved population of stars.

Masses: In the selected magnitude range, the galactic plane hosts an intrinsically more massive population, averaging to a mass slightly larger than the Sun, and the bulge is responsible for the peak of about 2.2 $M_\odot$. Higher latitudes, on the other hand, are dominated by low-mass stars where the masses average to slightly less than the Sun.

Absolute magnitudes: The more massive population in the galactic plane corresponds to intrinsically brighter stars, whereas higher galactic latitudes are, on average, dominated by fainter stars. The values correspond to the *average* absolute magnitude across the 1 deg^2 cell that is magnitude-selected, which is why the values are dominated by bright objects (the Malmquist bias).

Effective temperatures: The mean effective temperature in the galactic disc is dominated by a younger, hotter population, whereas the regions towards galactic poles are notably cooler, dominated by the late-type field stars.

Surface gravity: Given in *cgs* units (log g), high surface gravity (dwarfs) dominate the higher latitudes of the Galaxy, whereas low surface gravity (subgiants and giants) dominate the disc and most notably the bulge.

Interstellar extinction: The dust obscuration in the galactic plane is the main driver for the peak in extinction that averages to ~ 2.5 magnitudes (with large variations, of course: some local patches are completely obscured and others, such as Baade's window, are mostly transparent), and drops to substantially smaller (but not completely negligible) levels farther from the galactic plane.

Apparent magnitudes: The simulated sample spans the $Kp = 7$–17 magnitude range. In general, stellar population and interstellar extinction properties shape the distribution of magnitudes along the ecliptic. In the disc, obscuration wins out and results in a fainter sample; intermediate and higher latitudes are thus brighter. The region towards the galactic centre is again on the faint end, partly because of obscuration and partly because of the distance to the bulge.

Spectral types: The bulk of *Kepler* targets is in the *FGK* range, with earlier types found in the disc of the Galaxy and later types at intermediate and high latitudes. The effect of averaging across 1 deg^2 is particularly notable here, rendering the span of average spectral types essentially across the *G* range. The striking disparity near Baade's window is due to distinct populations – old, evolved population in the bulge and young, hot population in the disc.

Abundances: When compared to the Sun, most of the Galaxy is on average underabundant in metals, except for the bulge and the flaring thin disc. This is clearly evident in the abundance distribution, ranging from 20% underabundant ($[M/H] = -0.7$), typical of the thick disc population, to 25% overabundant ($[M/H] = +0.1$) towards the bulge.

With all this demonstrated variety along the ecliptic, the K2 mission is particularly well suited for population studies. Selected campaigns will probe inherently different populations and, for the first time, provide a nearly uninterrupted photometric coverage of tens of thousands of stars per field that will enable critical comparisons with, and calibrations of, the theoretical stellar population models.

K2 campaigns

Kepler is poised to observe ten fields in the next 2.5 years, which is the estimated time when the satellite runs out of fuel. As of this writing, only fields for campaigns 0 and 1 have been set; the remaining field locations are tentatively set but are subject to

https://doi.org/10.1017/S1473550414000329 Published online by Cambridge University Press

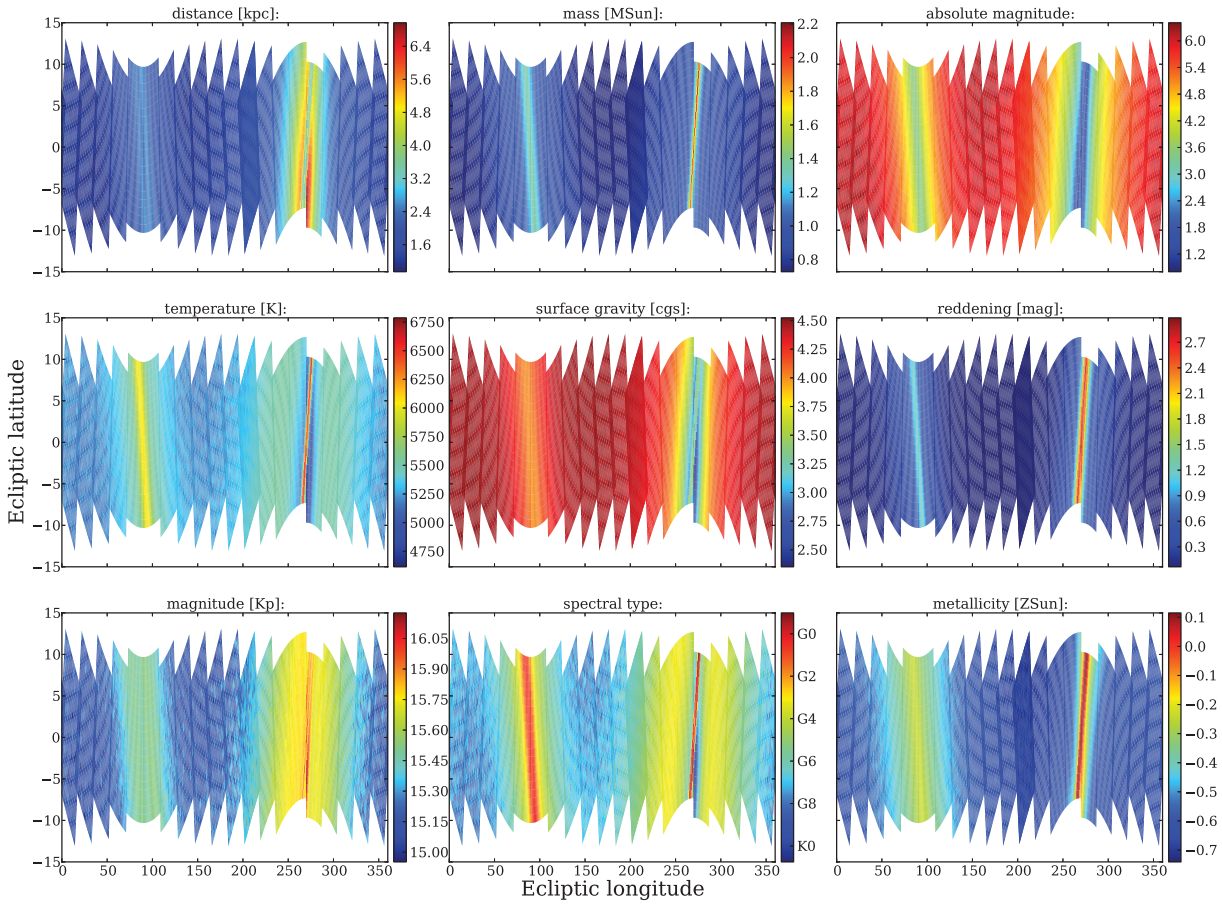

Fig. 2. Distributions of principal stellar parameters averaged over 1 deg^2 in the $Kp = 7$–17 range. All plots are given in ecliptic coordinates. Colour bars denote the corresponding parameter values. Note that the values do not span the whole range of stellar parameters, only the *average* values per 1 deg^2.

Table 1. *Proposed K2 campaigns. At the time of this writing, campaigns 0 and 1 have been set and the remaining campaigns are subject to change, depending on the engineering requirements and community feedback*

Campaign	End date	Centre α_{2000}	Centre δ_{2000}	Comments
0	2014-05-04	06 h 46 min 59.58 s	+21°22′47.1″	Near galactic anti-centre, M35, NGC2304
1	2014-07-23	11 h 37 min 55.65 s	+01°11′19.7″	North galactic cap
2	2014-10-14	16 h 34 min 43.63 s	−22°48′49.0″	Near galactic centre, M4, M80, M19
3	2015-01-05	22 h 21 min 06.01 s	−11°36′59.4″	South galactic cap, Neptune
4	2015-03-29	03 h 45 min 59.04 s	+18°07′49.7″	Pleiades (M45), Hyades, NGC1647
5	2015-06-20	09 h 19 min 02.66 s	+14°11′41.0″	Beehive (M44), M67
6	2015-09-11	14 h 01 min 11.20 s	−13°16′02.8″	North galactic cap
7	2015-12-03	19 h 34 min 16.22 s	−22°38′23.4″	Near galactic centre, NGC6717
8	2016-02-24	01 h 04 min 43.18 s	+05°11′52.2″	South galactic cap
9	2016-05-17	18 h 23 min 35.72 s	−24°12′12.8″	Galactic centre, Baade's window, M8

change if any scientific or engineering benefit from such a change is identified. Because of the engineering constraints discussed in the section 'Introduction', the roll angle of the satellite needs to be fine-tuned to provide stable pointing. The fields along the ecliptic may change by a few degrees to include high priority targets or clusters of targets; there is no plan to move off the ecliptic plane because then the roll angle will change much faster and the photometry will be much poorer. Furthermore, any adjustment in dates without the corresponding changes in all subsequent field dates would result in shorter campaigns. Table 1 summarizes the current and tentative K2 campaigns. For the remainder of this study we consider the first six campaigns and provide details for the remaining campaigns online at http://keplerEBs.villanova.edu/K2pops, where the information will be updated as soon as the campaign parameters are announced.

https://doi.org/10.1017/S1473550414000329 Published online by Cambridge University Press

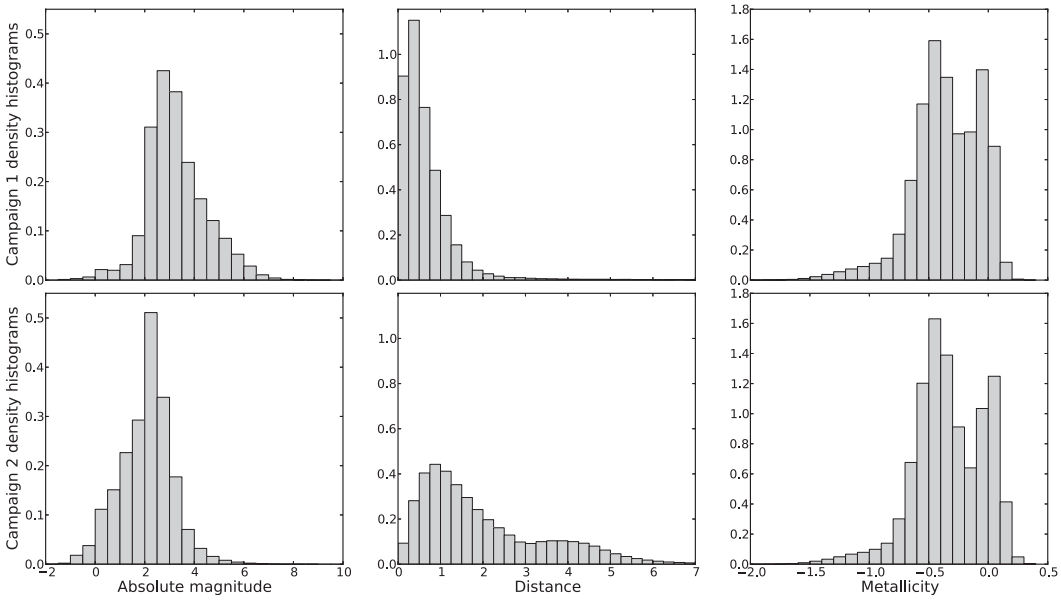

Fig. 3. Comparison of stellar populations for K2 campaigns 1 (north galactic cap) and 2 (galactic centre) in absolute magnitude, distance and metallicity. The histograms are density-normalized to facilitate comparison. The field at higher galactic latitudes is more abundant in intrinsically fainter stars that are closer to us (because of the $Kp = 7$–17 magnitude cut) and are predominantly underabundant. The field towards the galactic centre is dominated by brighter stars that are farther from us (because of the bulge giants) and feature distinct populations – underabundant in the disc and overabundant in the bulge. The main appeal of K2 is precisely this diversity in stellar populations.

Each campaign features a unique stellar population, with the most interesting targets listed in the Comments column of Table 1. We ran a detailed statistical check to estimate the expected field contents in terms of crowding and stellar populations. Figure 3 compares the populations in K2 campaigns 1 (north galactic cap) and 2 (galactic centre) in the distributions in absolute magnitude, distance and metallicity. Figure 4 provides an example for K2 campaign 1 that is scheduled to be observed in Summer 2014. The field is comparatively sparse in star counts brighter than $Kp \sim 17$, ranging between 500 and 700 per deg^2. In comparison, the original *Kepler* field featured over 7000 stars brighter than $Kp \sim 17$ per deg^2. Statistics plots for the remaining campaigns are available online at the aforementioned Villanova *Kepler* Eclipsing Binary Catalog site. Table 2 lists the number of stars of a given spectral type, including asymptotic giant branch (AGB) stars and white dwarfs (WD). While our simulation does not account for open clusters, these comprise only a few percent of the field-of-view and the number of targets in open clusters is commensurably small. The only exceptions are the Pleiades and the Hyades (Campaign 4), where our predictions likely underrepresent the young stellar population.

With *Kepler* ultimately being a planet hunting mission, we can provide a rough estimate of the planetary occurrence rates as well. As part of their eta-Earth ($\eta_\oplus$) project, Howard *et al.* (2010) observed a sample of 166 GK-type stars using the Keck/HIRES spectrograph and derived a power law that approximates the occurrence rates of close-in planets (orbital periods shorter than 50 days) as a function of planetary mass. This work was followed up for the *Kepler* planetary candidate sample (Howard *et al.* 2012) to find occurrence rates of $13.0 \pm 0.8\%$ for 2–4 $R_\oplus$ planets, $2.3 \pm 0.3\%$ for 4–8 $R_\oplus$ planets and $1.3 \pm 0.2\%$ for 8–38 $R_\oplus$ planets. The numbers are in agreement with a study by Fressin *et al.* (2013) that find a $16.5 \pm 3.6\%$ occurrence rate of 0.8–1.25 $R_\oplus$ planets around main sequence FGK stars with orbital periods shorter than 85 days. They do not find any significant dependence of 0.8–4 $R_\oplus$ planet occurrence rates on spectral type. While the majority of ~ 2500 *Kepler* planet candidates from the first 2 years of data have not been formally validated (even though the latest effort by Rowe *et al.* (2014) added 340 planetary systems with 851 planets to the validated count), probabilistic simulations have shown that a vast majority of these candidates are in fact planets (Morton & Johnson 2011; Fressin *et al.* 2013). Orbital periods of exoplanets are consistent with a flat distribution in log space (Dong & Zhu 2013), at least in the $\sim$ 1-day to the $\sim$ 100-day regime that is of most interest for K2 targets. We adopt these occurrence rates and the period distribution as definitive and use them to crudely estimate the number of transiting planets in each field.

For each star in the simulated field we draw an orbital period of a tentative planet from the flat log P distribution. Assuming that $M_{\rm planet} \ll M_*$, we compute the semi-major axis of the planetary orbit, assuming circular orbits. Orbital inclination is drawn from a uniform distribution and the orbit is projected onto the plane of sky. All systems that are sufficiently aligned with the line of sight to feature transits are counted, and their numbers are presented in Table 2. These crude numbers do not account for the low S/N cutoff or single event systems, nor do they reflect any instrumental window functions. They only serve as a rough guide to the expected number of planets in the

https://doi.org/10.1017/S1473550414000329 Published online by Cambridge University Press

Table 2. *A compendium of stellar types in the first 6 K2 campaigns. AGB are asymptotic giant branch stars, WD are white dwarfs, and TP are transiting planets in three size ranges: 2–4, 4–8 and 8–32* $R_\oplus$. *The table is divided into main sequence stars (top) and subgiants, giants and remnants (bottom). Planet occurrence rates apply only to dwarf stars. Note that these numbers correspond to the entire fields at the* Kp = *7–17 range, not just selected targets*

Campaign	O	B	A	F	G	K	M	AGB	WD	$TP_{2-4\,R_\oplus}$	$TP_{4-8\,R_\oplus}$	$TP_{8-32\,R_\oplus}$
Main sequence stars												
0	0	1640	16376	119056	177885	86731	11971	0	0	3464.5 ± 213.2	613.0 ± 80.0	346.5 ± 53.3
1	0	0	6	12264	18852	16699	7006	0	0	316.6 ± 19.5	56.0 ± 7.3	31.7 ± 4.9
2	0	26	523	206193	221858	105794	13113	0	0	4001.7 ± 246.3	708.0 ± 92.3	400.2 ± 61.6
3	0	0	20	21643	29222	23344	8631	0	0	483.3 ± 29.7	85.5 ± 11.2	48.3 ± 7.4
4	0	4	115	24175	45409	37481	9961	0	0	787.5 ± 48.5	139.3 ± 18.2	78.8 ± 12.1
5	0	2	26	15627	26040	23806	8243	0	0	439.5 ± 27.0	77.8 ± 10.1	44.0 ± 6.8

Campaign	O	B	A	F	G	K	M	AGB	WD
Subgiants, giants and remnants									
0	0	1250	15292	95791	54313	51664	1738	30	12
1	0	67	100	4864	3114	471	6	0	13
2	0	2534	4197	200750	330421	59162	613	18	11
3	0	152	213	9568	6002	889	13	0	10
4	0	30	119	11126	6681	2313	73	0	11
5	0	50	81	6585	3512	853	20	0	7

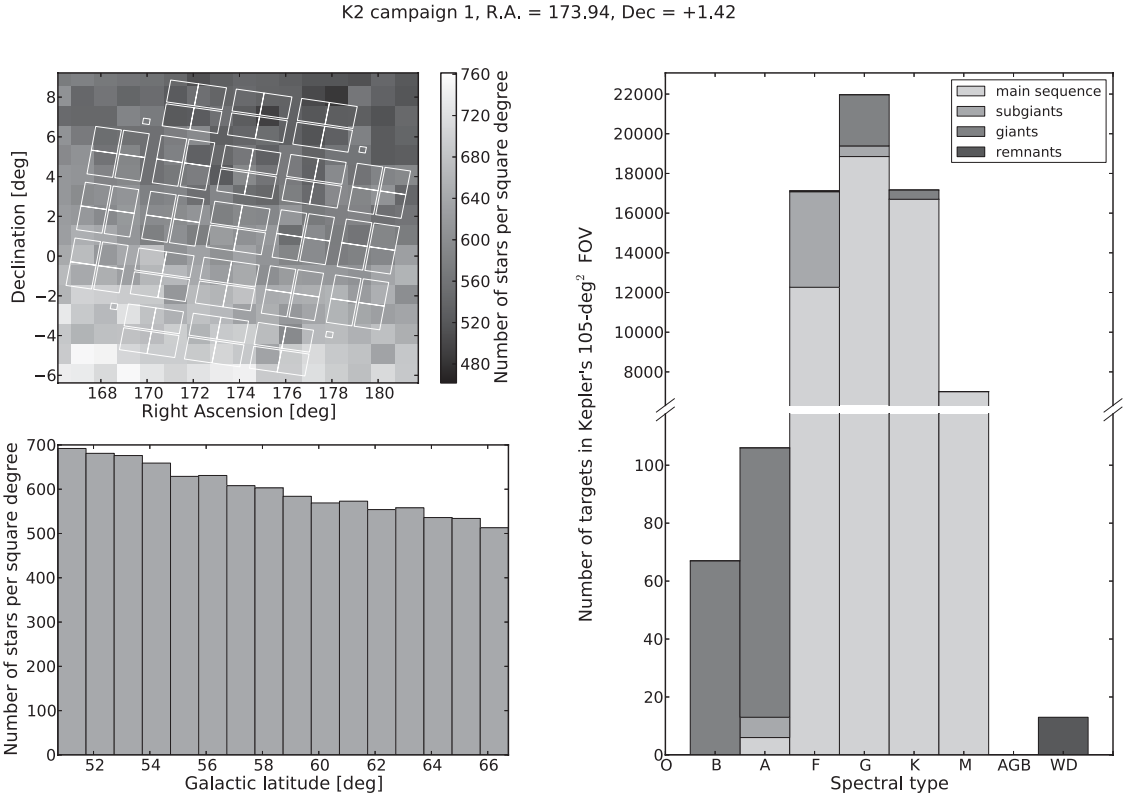

Fig. 4. K2 campaign 1 (α_{2000} = 11 h 37 min 55.65 s, δ_{2000} = +01°11′19.7″) statistics. Top left: the field-of-view superimposed on the star density map. This sparse field in terms of star counts features $\sim$ 500–700 stars per deg^2. Bottom left: star count per deg^2 as a function of galactic latitude. Right: star count as a function of spectral type, column-stacked by luminosity class. The sample consists of Kp = 7–17 stars.

field around all Kp = 7–17 stars, not only those selected as K2 targets.

A note on the role of K2 observations in calibrating stellar population models: target selection for K2 is based on community solicitation rather than any random draw, making a selection function highly biased. For that reason, the K2 sample holds limited promise for confronting theory with observations, and better datasets are available to serve as a testbed, most notably 2MASS, SDSS and, eventually, Gaia. The one exception is the use of asteroseismic techniques

https://doi.org/10.1017/S1473550414000329 Published online by Cambridge University Press

Table 3. *Crowding metric per K2 campaign. The values correspond to the (decimal) number of targets per* Kp = *12 star aperture with a 10, 5 and 3 px halo. Minimal, average and maximal values per K2 campaign are provided. The values are subject to change with the field centre and roll change*

	Min crowding			Average crowding			Max crowding		
Campaign	10 px	5 px	3 px	10 px	5 px	3 px	10 px	5 px	3 px
0	2.159	0.720	0.360	4.049 ± 1.198	1.350 ± 0.399	0.675 ± 0.200	5.496	1.832	0.916
1	0.351	0.117	0.058	0.410 ± 0.039	0.137 ± 0.013	0.068 ± 0.006	0.479	0.160	0.080
2	3.247	1.082	0.541	7.513 ± 3.785	2.504 ± 1.262	1.252 ± 0.631	15.857	5.286	2.643
3	0.508	0.169	0.085	0.658 ± 0.107	0.219 ± 0.036	0.110 ± 0.018	0.845	0.282	0.141
4	0.590	0.197	0.098	0.891 ± 0.227	0.297 ± 0.076	0.148 ± 0.038	1.323	0.441	0.220
5	0.420	0.140	0.070	0.553 ± 0.091	0.184 ± 0.030	0.092 ± 0.015	0.732	0.244	0.122

(Miglio *et al.* 2009) to compare model density laws with observations, and to determine surface gravity; the latter constrains the star formation history via the age distribution that can be deduced from stellar evolution models. For those reasons we use the BGM as 'ground truth', keeping in mind the uncertainties and deficiencies discussed earlier, to produce a description of bulk properties of the K2 stellar populations.

Crowding and contamination

Kepler is designed as a planet hunting mission, so it is crucial to understand and estimate the amount of crowding in the field and contamination due to third light. Eclipsing binary stars have been the main culprit for false positives: signals in light curves that resemble those of planetary transits (Fressin *et al.* 2013). Because of third light dilution, the depths of stellar eclipses are quenched to planetary transit levels and complex approaches and/or follow-up spectroscopic campaigns are necessary to validate true planets (Torres *et al.* 2011).

Based on the engineering run in the ecliptic (Howell *et al.* 2014), the K2 mission performs only marginally poorer than the original setup: the PSF is up to 5% larger, and the main cause of photometric degradation is the solar-induced drift of the instrument. This drift is corrected by firing the on-board thrusters at regular time intervals, so even though per-field PSF remains largely unchanged, the apertures are enlarged to account for this 1–2 pixel drift. The initial campaign serves primarily as an engineering run, and all apertures are enlarged by adding a 10-pixel (px) 'halo' around them, to add ample margins for initial pointing uncertainties and drift offsets during the campaign. This will likely be reduced to a 5-px 'halo' for campaign 1, and the aperture sizes will be further optimized for subsequent campaigns based on the engineering data. Figure 5 depicts new aperture sizes (in pixels) for a 10 px, a 5 px and a 3 px halo. This consideration, coupled with the decreased telemetry rate with the satellite that is currently ~ 0.5 AU from the Earth, the increased temporal baseline (and, with it, on-board data storage requirements) from 30 to 81 days between data downlinks, and a poorer data compression rate because of the target motion, requires a significant reduction in the number of targets observed: only 10 000 to 20 000 for campaigns 0 and 1, and $\sim$ 30 000 for the subsequent campaigns, compared with the 160 000 targets of the original mission.

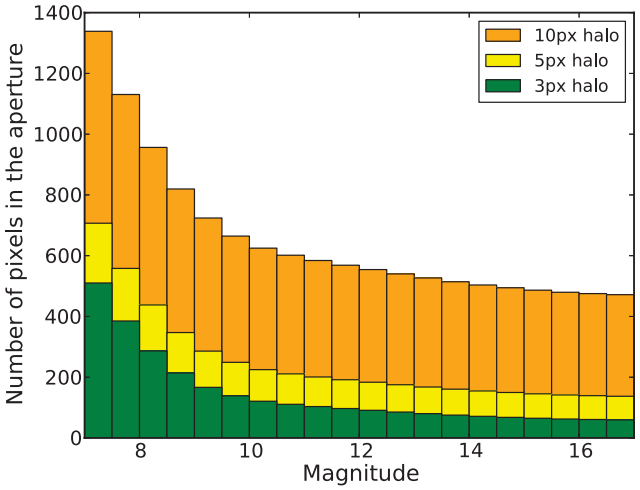

Fig. 5. Aperture size as a function of magnitude. Three cases are presented: optimal aperture size for the original *Kepler* field augmented by a 10 px halo (orange), a 5 px halo (yellow) and a 3 px halo (green). A 10 px halo is used for K2 campaign 0, 5 px halo will likely be used for campaign 1, and a 3 px halo might be used for subsequent campaigns, pending the results from the first two campaigns.

With larger apertures, crowding becomes an even more important issue. As a crowding metric, we choose a $Kp = 12$ magnitude star. The aperture size that corresponds to such a star is 554, 184 and 92 px for 10, 5 and 3 px halos, respectively (cf. Fig. 5). Given the *Kepler* pixel size of $4'' \times 4''$, the corresponding areas are 2.46, 0.82 and 0.41 arcmin^2. The star density per deg^2 (Fig. 1) thus needs to be rescaled appropriately and we can use that as a metric for crowding in different fields. Table 3 lists these values for all K2 campaigns.

Conclusions

The K2 mission concept promises to yield invaluable data similar in nature to the original *Kepler* mission, and akin to the upcoming Transiting Exoplanet Survey Satellite (TESS; Ricker *et al.* 2010). With $\sim$ 81 days on a single field, K2 will probe inherently different stellar populations and, contingent on NASA HQ approval and continued funding for 2.5 years, provide photometric coverage of over 250 000 stars. This paper provides a guide to expected stellar populations, crowding

https://doi.org/10.1017/S1473550414000329 Published online by Cambridge University Press

and planetary occurrence rates along the ecliptic based on the improved Besançon model simulations.

This work does not include multiple stellar systems; these may be important since the evolutionary channels that correspond to multiples can be sufficiently different to affect the overall stellar population. That said, no significant difference was observed in the eclipsing binary and single star population in the *Kepler* field of view (Slawson *et al.* 2011), so even though K2 will sample a much larger span of galactic latitudes, the effect will likely be limited to 5–10%. Likewise, the absence of open clusters in the simulation might cause an underrepresented sample of young stars in the campaigns containing M35, the Pleiades, the Hyades and the Praesepe, but targets in open clusters are very limited in number across all campaigns ($<1\%$), hence the presented bulk properties remain unaffected.

Understanding stellar binarity and multiplicity is the next step in the study of K2 campaigns. From *Kepler* observations of 2615 eclipsing and ellipsoidal binary stars (Prša *et al.* 2011; Slawson *et al.* 2011) that are essentially complete to $P \sim 500$ days, we can derive the underlying orbital period and eccentricity distributions. We do this by correcting for the bias using Bayesian methods outlined in Hogg *et al.* (2010). From the underlying distributions we simulate binary and multiple stars by applying the observed occurrence rates from Raghavan *et al.* (2010) to the Besançon sample of stars that are grouped into multiple systems under the constraints of coevality and equal metallicity. These systems are then statistically examined for eclipses and eclipse timing variations. This in-depth analysis requires a substantial discussion that is beyond the scope of the present work, and will be discussed in the follow-up paper.

An alternative BGM (Czekaj *et al.* 2014) will be used in the future, which presents a better fit for bright stars ($V<12$) using more recent stellar evolution models and atmosphere models, and introduces a specific treatment of the binary star population. This model has suitable flexibility to test alternative star formation history and initial mass function assumptions.

Inherently different stellar (and planetary) populations along the ecliptic provide us with an opportunity to study population differences as a function of galactic latitude. Table 2 lists the expected numbers of main sequence stars and giants for each campaign, attesting to the variety of objects for which K2 will provide ultraprecise, long temporal baseline photometry. In combination with Gaia (de Bruijne 2012) that has recently seen first light, TESS that is scheduled to launch in 2017, and Plato (Catala 2009) that has been selected as the third ETS medium-class science mission, the K2 dataset will be a gold mine for stellar and planetary astrophysics.

Acknowledgements

The authors acknowledge support through NASA Kepler PSP grant NNX12AD20G, and thank Kyle Conroy, Joshua Pepper, Tabetha Boyajian, Keivan Stassun, Pieter Degroote, Kelly Hambleton, Mike Haas and William Borucki for useful discussions and suggestions. BGM simulations were executed on computers from the Utinam Institute of the Université de Franche-Comté, supported by the Région de Franche-Comté and Institut des Sciences de l'Univers (INSU).

References

Arenou, F. (2011). In *American Institute of Physics Conference Series*, Vol. 1346, ed. Docobo, J.A., Tamazian, V.S. & Balega, Y.Y., pp. 107–121.
Baglin, A. (2003). *Adv. Space Res.* **31**, 345.
Batalha, N.M., Rowe, J.F., Bryson, S.T. *et al.* (2013). *Astrophys. J. Suppl.* **204**, 24.
Borucki, W.J., Koch, D., Basri, G. *et al.* (2010). *Science* **327**, 977.
Burke, C.J., Bryson, S.T., Mullally, F. *et al.* (2014). *Astrophys. J. Suppl.* **210**, 19.
Cardelli, J.A., Clayton, G.C. & Mathis, J.S. (1989). *Astrophys. J.* **345**, 245.
Catala, C. (2009). *Exp. Astron.* **23**, 329.
Chaplin, W.J., Kjeldsen, H., Christensen-Dalsgaard, J. *et al.* (2011). *Science* **332**, 213.
Czekaj, M.A., Robin, A.C., Figueras, F., Luri, X. & Haywood, M. (2014). A&A **564**, A102.
de Bruijne, J.H.J. (2012). *Astrophys. Space Sci.* **341**, 31.
Dong, S. & Zhu, Z. (2013). *Astrophys. J.* **778**, 53.
Fressin, F., Torres, G., Charbonneau, D. *et al.* (2013). *Astrophys. J.* **766**, 81.
Gaulme, P., McKeever, J., Rawls, M.L. *et al.* (2013). *Astrophys. J.* **767**, 82.
Girardi, L., Groenewegen, M.A.T., Hatziminaoglou, E. & da Costa, L. (2005). *Astron. Astrophys.* **436**, 895.
Hogg, D.W., Myers, A.D. & Bovy, J. (2010). *Astrophys. J.* **725**, 2166.
Howard, A.W., Marcy, G.W., Johnson, J.A. *et al.* (2010). *Science* **330**, 653.
Howard, A.W., Marcy, G.W., Bryson, S.T. *et al.* (2012). *Astrophys. J. Suppl.* **201**, 15.
Howell, S.B., Sobeck, C., Haas, M. *et al.* (2014). arXiv:1402.5163.
Huber, D., Chaplin, W.J., Christensen-Dalsgaard, J. *et al.* (2013). *Astrophys. J.* **767**, 127.
Marshall, D.J., Robin, A.C., Reylé, C., Schultheis, M. & Picaud, S. (2006). *Astron. Astrophys.* **453**, 635.
Miglio, A., Montalbán, J., Baudin, F. *et al.* (2009). *Astron. Astrophys.* **503**, L21.
Morton, T.D. & Johnson, J.A. (2011). *Astrophys. J.* **738**, 170.
Ng, Y.K., Bertelli, G., Chiosi, C. & Bressan, A. (1997). *Astron. Astrophys.* **324**, 65.
Papics, P.I. (2013). *PhD Thesis*, Instituut voor Sterrenkunde, KU Leuven, Celestijnenlaan 200D, B-3001 Leuven, Belgium.
Prša, A., Batalha, N., Slawson, R.W. *et al.* (2011). *Astron. J.* **141**, 83.
Raghavan, D., McAlister, H.A., Henry, T.J. *et al.* (2010). *Astrophys. J. Suppl.* **190**, 1.
Reylé, C., Marshall, D.J., Robin, A.C. & Schultheis, M. (2009). *Astron. Astrophys.* **495**, 819.
Ricker, G.R., Latham, D.W., Vanderspek, R.K. *et al.* (2010). In Bulletin of the American Astronomical Society, vol. 42, American Astronomical Society Meeting Abstracts #215, #450.06.
Robin, A.C., Reylé, C., Derrière, S. & Picaud, S. (2003). *Astron. Astrophys.* **409**, 523.
Robin, A.C., Reylé, C., Fliri, J., Czekaj, M., Robert, C.P. & Martins, A.M.M. (2014). arXiv. 1406, 5384 (has not appeared in print yet).
Robin, A.C., Marshall, D.J., Schultheis, M. & Reylé, C. (2012). *Astron. Astrophys.* **538**, A106.
Rowe, J.F., Bryson, S.T., Marcy, G.W. *et al.* (2014). *Astrophys. J.* **784**, 45.
Sharma, S., Bland-Hawthorn, J., Johnston, K.V. & Binney, J. (2011). *Astrophys. J.* **730**, 3.
Slawson, R.W., Prša, A., Welsh, W.F. *et al.* (2011). *Astron. J.* **142**, 160.
Torres, G., Fressin, F., Batalha, N.M. *et al.* (2011). *Astrophys. J.* **727**, 24.
Vallenari, A., Bertelli, G., Bressan, A. & Chiosi, C. (1999). *Balt. Astron.* **8**, 147.
Westera, P., Lejeune, T. & Buser, R. (1999). In *Astronomical Society of the Pacific Conference Series, vol. 192*, ed. I. Hubeny, S. Heap, & R. Cornett, *Spectrophotometric Dating of Stars and Galaxies*, p. 203.

https://doi.org/10.1017/S1473550414000329 Published online by Cambridge University Press